Journal of Power Sources 181 (2008) 56–61

Contents lists available at ScienceDirect

Journal of Power Sources

journal homepage: www.elsevier.com/locate/jpowsour

Phase transitions and phase decomposition of $La_{1-x}Sr_xCoO_{3-\delta}$ in low oxygen partial pressures

James Ovenstone, Jeffery S. White, Scott T. Misture*

Kazuo Inamori School of Engineering, Alfred University, Alfred, NY 14802, United States

ARTICLE INFO

Article history:
Received 11 February 2008
Received in revised form 5 March 2008
Accepted 16 March 2008
Available online 22 March 2008

Keywords:
Solid oxide fuel cell
Cathode
LSC
Brownmillerite
Vacancy ordering

ABSTRACT

High-temperature X-ray diffraction has been used to investigate the phase stability of lanthanum strontium cobalt oxide (LSC) for a range of materials with the formula $La_{1-x}Sr_xCoO_{3-\delta}$ ($x = 0.7$, 0.4, and 0.2). The stability of LSC increases with La content in low oxygen partial pressures at high temperature. Oxygen vacancy ordering has been observed for all three compositions in either low oxygen pressure or under reducing gas, as evidenced by the formation of the brownmillerite phase. The crystal structure of the vacancy-ordered phase was determined using Rietveld analysis of synchrotron X-ray diffraction data. The decomposition products under low oxygen pressure and in reducing conditions have been identified and characterized, including the phase transition and thermal expansion of the primary decomposition products, $LaSrCoO_4$ and $LaSrCoO_{3.5}$.

1. Introduction

Lanthanum strontium cobalt oxide (LSC, $La_{1-x}Sr_xCoO_{3-\delta}$) has been the subject of significant research interest as a colossal magnetoresistive material [1–3], for use as oxygen separation membranes [4–7] and in solid oxide fuel cell cathodes [7–11]. One common SOFC cathode material is strontium-doped lanthanum magnetite (LSM), which is an excellent electronic conductor and oxygen reduction catalyst [12,13]. At the lower operating temperatures of intermediate-temperature SOFCs (800 °C and below), however, the low conductivity of LSM reduces efficiency.

LSC, unlike LSM, is a mixed conductor and the oxygen sublattice is of critical importance in its conductivity. Many studies of the oxygen nonstoichiometry, magnetic properties, conductivity, and thermal expansion have been published, and the electrical behavior is well understood [6,14–26]. Little, however, has been published concerning the phase stability under conditions of low oxygen activity.

In a recent study, Chen [15] used dilatometry to track changes in the length of monolithic LSC bars as a function of pO_2. Their results clearly demonstrated isothermal volumetric drifting in low pO_2 static atmospheres, where a stable state was not reached even after a number of days. They suggested that the drift was related to local rearrangement of cations to obtain a structure containing microdomains, or possibly phase separation, rather than simply the result of a change in the oxidation state of the B site cation.

A very recent review by Petrov et al. [25] includes phase diagrams for LSC and related materials and describes decomposition mechanisms for LSC. However, the authors did not detect vacancy-ordered forms of LSC. Two studies of $La_{1-x}Sr_xCoO_{3-\delta}$ with $x = 0.5$ (LSC55) showed that $(SrLa)_2CoO_4$ and a cobalt-rich oxide form from LSC under $pO_2 = 0.012$ atm [20,31].

Microdomains appear to be a common structural feature of LSC, LSCF, and $SrCoO_{3-d}$, having been observed directly with electron microscopy by van Doorn and Burggraaf [6], Caciuffo et al. [27], Bucher et al. [14], Klie et al. [28], Bangert et al. [29], and Stemmer et al. [30]. Magnetic ordering is also a sensitive probe of the materials at the size scale of a few unit cells, and several studies suggest cation clustering in LSC [21,27].

Several papers suggest that vacancy-ordered phases are formed under conditions of low oxygen activity. For example, studies of LSC [27], Ga-substituted LSC [5], LSCF [32], SCF [33,34], and SC [35] all point to vacancy-ordered phases but do not include structural information. The work of Liu et al. [33] showed that SCF undergoes the transition to the ordered brownmillerite through a two-phase region that is dependent upon temperature and oxygen vacancy concentration. The brownmillerite takes the form of $(La,Sr)_2Co_2O_5$, presumably, by ordering oxygen vacancies in alternate layers of cations.

The only direct observation of vacancy ordering in LSC was reported by James et al. [36]. Using neutron diffraction, these authors found a very subtle ordering of oxygen vacancies, resulting

* Corresponding author. Tel.: +1 607 871 2438; fax: +1 607 871 2354.
E-mail address: misture@alfred.edu (S.T. Misture).

0378-7753/$ – see front matter © 2008 Elsevier B.V. All rights reserved.
doi:10.1016/j.jpowsour.2008.03.033

in a tetragonal cell that is double the perovskite cell along the *c*-axis for the high La end of the series, $La_{0.9}Sr_{0.1}CoO_{3-\delta}$. Unfortunately, no additional crystal structures have been reported, and no details concerning the structures and stability ranges of the brownmillerite form of vacancy-ordered LSC are available.

2. Experimental

LSC powders were obtained from Praxair Ltd. and used as-received. High-temperature X-ray diffraction was carried out using a Siemens θ-θ D500 diffractometer equipped with a Braun position sensitive detector and high-temperature furnace of custom design with Co Kα radiation [37]. Gas flows were controlled using two Omega FMA5400/5500 mass flow controllers, and oxygen concentrations measured using a Thermox CG1000 oxygen analyzer on the outlet side of the diffraction furnace. The high-temperature XRD experiments were carried out using a heating rate of 60 °C min^{-1}, with measurements made every 25 °C. Measurements were made over the 2θ range 20–130° 2θ using a scan rate of 10° min^{-1}. SEM was carried out using an FEI Quanta 200F field emission environmental SEM equipped with a hot stage, backscatter detector, and EDX detector.

Reagent grade powders of La_2O_3, $SrCO_3$, and Co_3O_4 were used to synthesize pure $SrLaCoO_4$ via solid-state synthesis. The precursor oxides were vibratory milled in a McCrone Micronising Mill with alumina media, then dried and pressed into 1.9 cm diameter by 0.5 cm thick pellets at 27.6 MPa. The pellets were sintered in air at 1350 °C for 4 h with a ramp rate of 500 °C per hour in a platinum crucible and allowed to furnace cool.

One ambient-temperature XRD pattern of the vacancy-ordered LSC phase was measured using synchrotron radiation at the National Synchrotron Light Source at Brookhaven National Laboratory. Beamline X14A was used to perform a reflection-geometry powder diffraction experiment using a Ge111 analyzer crystal and wavelength = 0.7336 Å. Rietveld analysis was performed using Topas (Bruker-AXS) Version 4. The specimen was prepared by annealing LSC37 under flowing H_2 for 2 h at 275 °C and quenching.

3. Results and discussion

The SEM micrographs in Fig. 1 show the three starting powders, LSC37, LSC64, and LSC82. The LSC37 powder appears to have a bimodal size distribution, with larger particles in the range of 1 μm and smaller particles of ~100 nm. The LSC64 and LSC82 powders have particle sizes on the order of 500 nm. Ambient-temperature XRD data showed all powders to be phase-pure LSC.

Fig. 2 shows the *in situ* diffraction data for $La_{0.3}Sr_{0.7}CoO_{3-\delta}$ (LSC37) powder heated and cooled under $pO_2 = 10^{-5}$ atm. LSC clearly transforms from cubic symmetry with random oxygen vacancies to a new form that contains many additional diffraction lines as the temperature increases up to 800 °C. The phase transition shown in Fig. 5 can be attributed to oxygen vacancy ordering because the diffraction pattern of the high temperature form is characteristic of the brownmillerite structure that has ordered oxygen vacancies. The oxygen vacancy ordering is slow and occurs over a broad temperature range, not unlike other order–disorder transitions. It is interesting to note that the ordering is reversible, and that the ordered phase partially disorders on cooling until the structure is frozen in at ~300 °C.

Rietveld analysis of the initial XRD data for the LSC37 vacancy-ordered specimen quenched to room temperature suggested that the specimen contained ~70 wt% of the ordered phase. A high-resolution synchrotron powder pattern was used to clarify the unit cell symmetry, although neutron diffraction would be ideal to describe the oxygen sublattice.

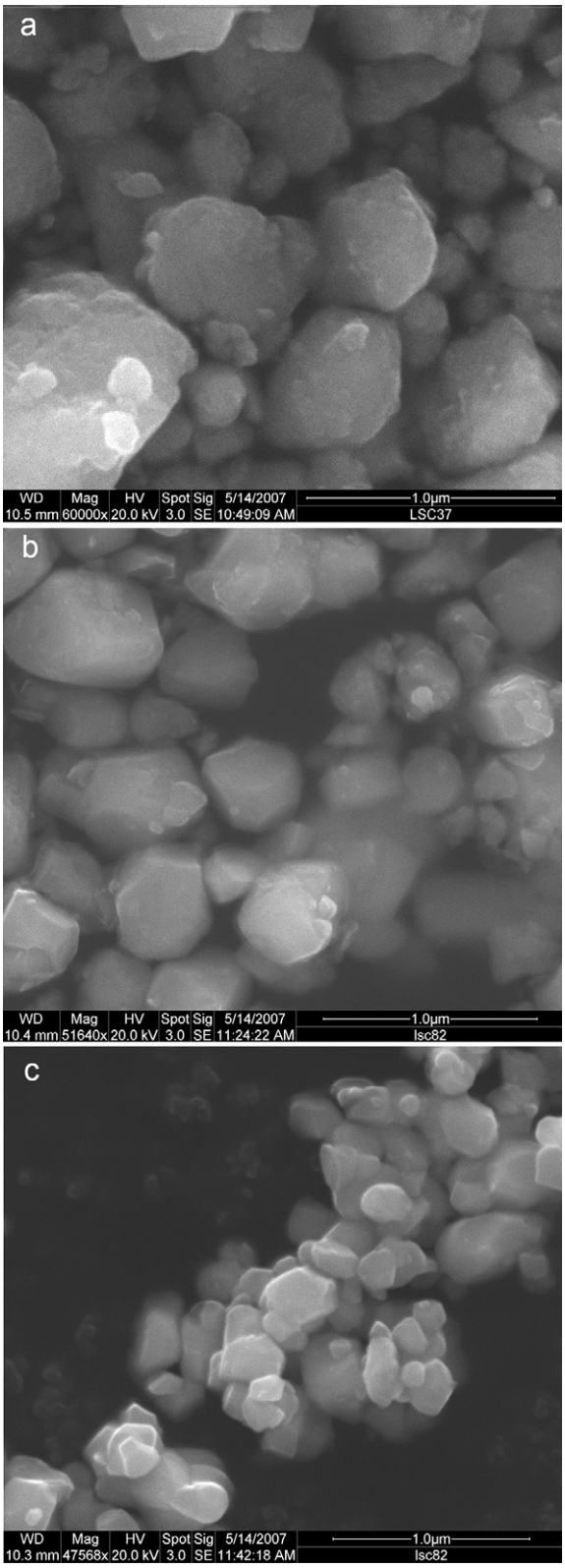

Fig. 1. SEM micrographs of (a) LSC37, (b) LSC64, and (c) LSC82 powders.

A review of reference databases including the powder diffraction file [38] and the inorganic crystal structure database [39] resulted in several possible transition-metal oxide phases matching the diffraction pattern for the vacancy-ordered phase. The reported space groups of the similar brownmillerite-type phases include

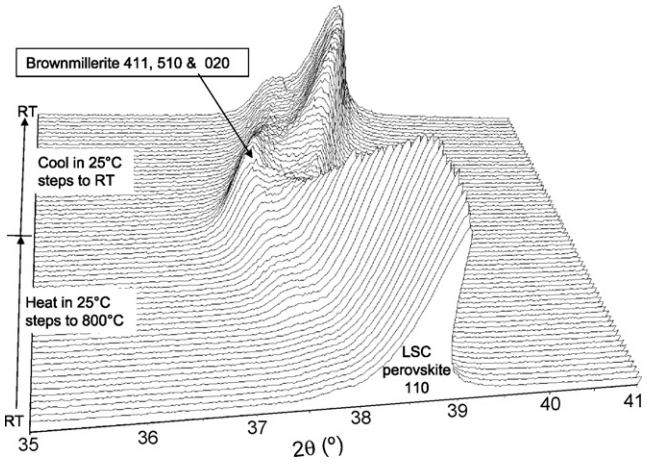

Fig. 2. *In situ* X-ray diffraction data (Co radiation, λ = 1.79 Å) for LSC37 heated to 800 °C and then cooled to room temperature under $pO_2 = 10^{-5}$ atm. Data are shown at 25 °C intervals.

I*ma*2, P*nma*, and I*mma*. The reference data for the lowest-symmetry structure, $Sr_2Co_2O_5$, I*ma*2 [40] provided the best match to the measured intensities, and was used as the starting model in the refinement.

During refinement, the model was tested as a random solid solution of La and Sr on the Sr sites. No ordering was detected, and subsequent attempts to refine the La and Sr positions independently did not improve the refinement results. Therefore, the La and Sr positions were constrained to occupy the same site, and their isotropic displacement parameters were constrained to be the same. The final refinement is shown in Fig. 3, with the structure shown in Fig. 4 and the structural and refinement details in Tables 1 and 2.

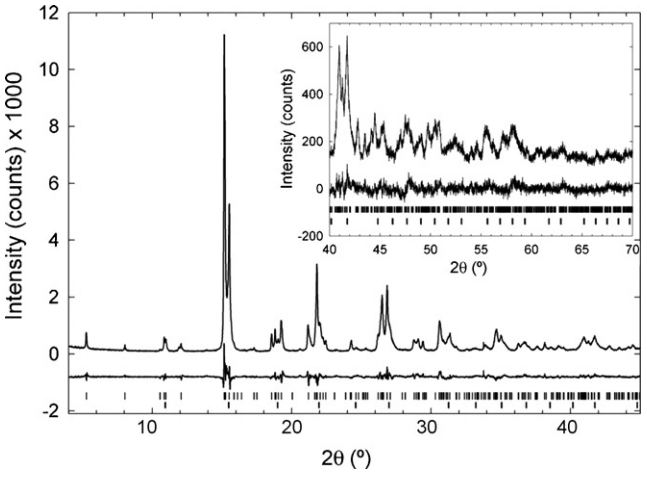

Fig. 3. Rietveld analysis of partially vacancy-ordered LSC37 at room temperature. Observed and difference patterns are shown, with tick marks for vacancy-ordered LSC (top) and cubic LSC (bottom). Synchrotron radiation, λ = 0.7336 Å.

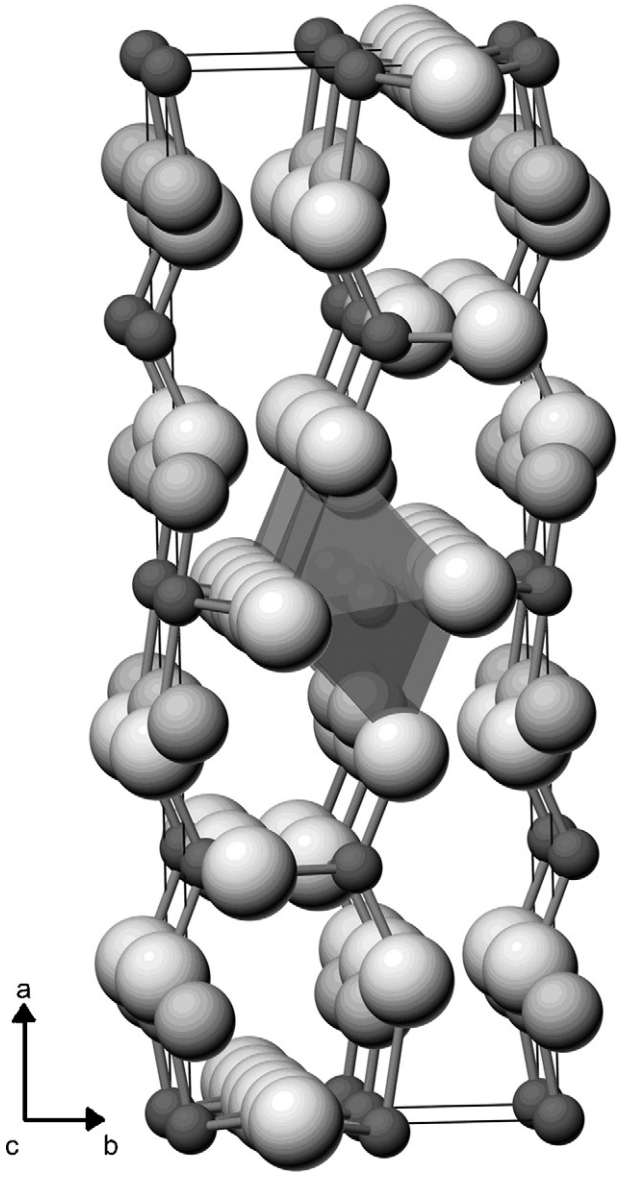

Fig. 4. Refined structure of vacancy-ordered LSC37.

Although the cation positions in $La_{0.3}Sr_{0.7}CoO_{2.5}$ are shifted slightly from those in the starting model for $Sr_2Co_2O_5$, all of the bond lengths remain reasonable for both the tetrahedral and octahedral Co polyhedra. The O3 position was successfully refined, to accommodate a shift in the Co2 position that resulted in a slightly elongated Co2–O3 bond length. The average bond lengths in the

Table 1
Data collection details, crystal data and structure refinement parameters for $La_{0.3}Sr_{0.7}CoO_{2.5}$

Formula	$La_{0.3}Sr_{0.7}CoO_{2.5}$
Specimen dimensions	Powder, reflection geometry, 3 mm thick
Space group	*Ima*2
Unit cell (25 ± 2 °C)	$a = 15.9536\ (7)$, $b = 5.5405\ (2)$, $c = 5.4339\ (2)$ Å and volume = 480.31 (3) Å^3
Calculated linear absorption coefficient (cm^{-1})	315
Mass density (g cm^{-3})	5.59
Wavelength	0.73363 Å
Data range	$4 < 2\theta < 85°$; $10 < d < 0.54$ Å
Weighted residual, Rwp	9.6%
GOF	1.5

Table 2
Atomic coordinates, occupancies, and equivalent isotropic displacement parameters for $La_{0.3}Sr_{0.7}CoO_{2.5}$

Site	*x*	*y*	*z*	Occupancy	*B* (equiv.)
Co1	0	0	0	1	0.53 (6)
Co2	1/4	0.05834 (60)	0.0268 (21)	1	0.55 (9)
Sr/La	0.10914 (8)	0.50843 (35)	0.0020 (18)	0.7	0.72 (4)
La/Sr	0.10914 (8)	0.50843 (35)	0.0020 (18)	0.3	0.72 (4)
O1	0.0141	0.2475	0.2497	1	1
O2	0.1429	0.5683	0.4744	1	1
O3	1/4	0.1429 (34)	0.3793 (45)	1	1

CoO_4 and CoO_6 polyhedra in $La_{0.3}Sr_{0.7}CoO_{2.5}$ are within 0.004 Å of those in $Sr_2Co_2O_5$ and are therefore not listed separately herein.

Using the structure model for the vacancy-ordered phase, Rietveld analysis was used to quantify the phase assemblage for three compositions of LSC as a function of oxygen activity and temperature. In the case of LSC37, oxygen vacancy ordering at intermediate temperatures was followed by disordering at higher temperature to form a defect perovskite, so that the ordering sequence follows: disordered → ordered → disordered.

Fig. 5 shows the results for LSC37, demonstrating that the transition to the brownmillerite phase begins at ~300 °C under 10^{-4} and 10^{-3} atm oxygen, and is not detected until ~400 °C under 10^{-3} atm oxygen. The extent of conversion to the brownmillerite phase is of course a function of the oxygen activity, composition, temperature, and time. Liu et al. [33] showed that SCF goes through a two-phase region bounded by the defect perovskite at higher oxygen content and the brownmillerite at lower oxygen content and showed that the ordering reaction is slow, probably a result of Fe and Co rearrangement. The results shown in Fig. 5 suggest that LSC37 also passes through a two-phase region because disordering occurs before vacancy ordering has gone to completion. Although we have probably not equilibrated the specimens during the *in situ* XRD measurement, the extent of conversion to the ordered phase trends with oxygen partial pressure. As shown in Fig. 5, the conversion to the vacancy-ordered phase reaches 48, 46, 22, and 16 wt% for 10^{-5}, 10^{-4}, 10^{-3}, and 10^{-2} atm oxygen, respectively.

Also shown in Fig. 5 is the trend of high-temperature oxygen vacancy disordering, where lower oxygen activity raises the disordering temperature. Vacancy disordering at high temperature has been detected in other cobaltites, for example LSCF which also shows a transition from the ordered brownmillerite phase to disordered perovskite structure on heating [32]. $Sr_2Co_{1.6}Fe_{0.4}O_5$ and $Ba_2In_2O_5$ are additional examples of ionic and mixed conductors

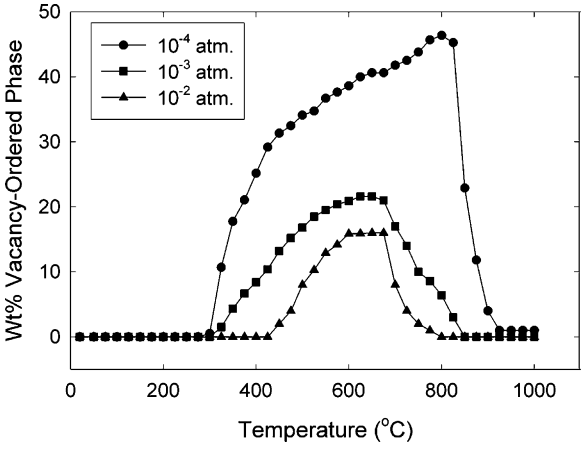

Fig. 5. Fraction of vacancy-ordered LSC37 as a function of temperature for $pO_2 = 10^{-4}$, 10^{-3}, and 10^{-2} atm. Error bars are slightly larger than the symbols and not shown.

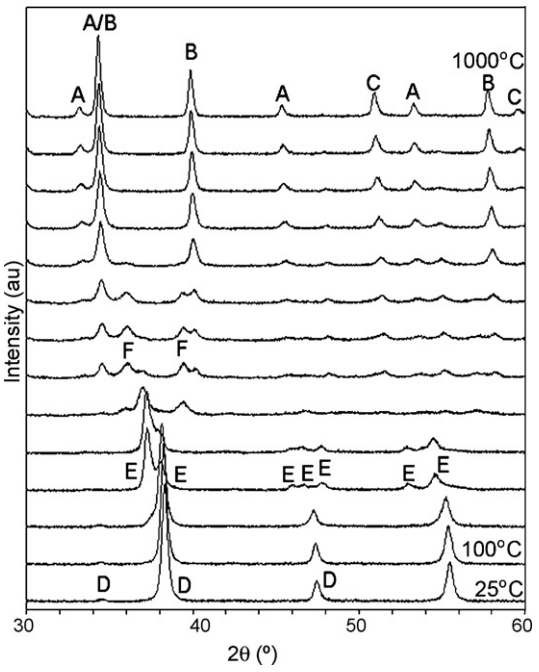

Fig. 6. *In situ* X-ray diffraction data (Co radiation, λ = 1.79 Å) for LSC37 heated in 4% hydrogen. Data are shown in steps of 75 °C. A = La_2O_3, B = SrO, C = Co, D = LSC37, E = vacancy-ordered LSC37 and F = $SrLaCoO_4$.

that display transitions to disordered, cubic polymorphs on heating [34,38].

LSC37 becomes unstable beginning at ~925 °C and $pO_2 = 10^{-5}$ atm and at 1000 °C under $pO_2 = 10^{-4}$ atm. In both cases, LSC37 decomposes to form $(La,Sr)_2CoO_4$ and CoO, in agreement with earlier work on LSC55 [20,31]. The $(La,Sr)_2CoO_4$ phase has been reasonably well characterized, having found application as an oxidation catalyst [39], and being related to the SOFC cathode materials. It crystallizes in the K_2NiF_4 structure type and is the $n = 1$ member of the Ruddlesden–Popper series.

Extending the atmosphere to reducing conditions, 4% H_2 in N_2, results in further phase decomposition. Fig. 6 shows the phase evolution for LSC37 heated under 4% H_2. Initial formation of the vacancy-ordered phase occurs at 200 °C. At 350 °C decomposition begins as CoO begins to form, together with a small amount of SrO and $(La,Sr)_2CoO_{3.5}$. The latter phase is interesting in that it is the reduction product of $LaSrCoO_4$ [41] and is described in more detail below.

From 675 °C upward, the final set of products begins to form from LSC37, yielding La_2O_3, SrO, and Co metal. These remain stable up to 1000 °C, and upon cooling to room temperature. On exposure to air, however, even at room temperature, the products decompose to a complex series of hydroxides and carbonates. The decomposition sequence is completely reversible, however; reheating the reduced products in air at 1000 °C yields pure LSC37 within a few minutes.

Heyward and Rosseinsky determined the crystal and magnetic structures of $LaSrCoO_{3.5}$ [41], but details of the phase transition and thermal expansion are not available. To better understand the oxygen deficient phase, we prepared pure $LaSrCoO_4$ and measured the reduction to $LaSrCoO_{3.5}$ *in situ*. The result of reduction under 4% H_2 is shown in Fig. 7, suggesting a direct transition to the reduced phase with no intermediates, beginning at 380 °C. Further heating results in complete transition to $LaSrCoO_{3.5}$ by ~450 °C, followed by decomposition beginning at ~600 °C. $LaSrCoO_{3.5}$ remained stable upon cooling at ~100 °C min^{-1} to room temperature, and was

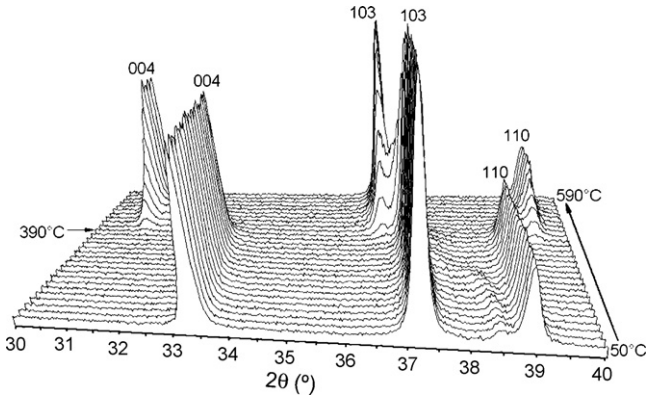

Fig. 7. High-temperature diffraction data (Co radiation, $\lambda = 1.79$ Å) for $LaSrCoO_4$ heated under 4% H_2. Transition from $LaSrCoO_4$ to $LaSrCoO_{3.5}$ begins at 390 °C. Data are shown at 20 °C intervals.

completely reversible, transforming back to the fully oxidized phase on reheating in air.

Tracking the unit cell parameters of the tetragonal cell as a function of temperature under air, 10^{-5} atm oxygen and 4% H_2 yields the result in Fig. 8. Using the unit cell volume expansion to estimate the linear coefficient of thermal expansion (CTE) for $LaSrCoO_4$ results in a value of 22.3 ppm K^{-1} (RT to 850 °C) and 20.3 ppm K^{-1} (RT to 600 °C). The CTE for the oxygen-deficient $LaSrCoO_{3.5}$ is substantially lower over its stability range, 13.4 ppm K^{-1} (RT to 600 °C).

The phase decomposition sequence was also determined for LSC64 and LSC82 to probe the effects of the A-site chemistry on stability. LSC64 is rhombohedral at room temperature and transforms to cubic symmetry on heating in air. As with LSC37, LSC64 is stable in 1% O_2, but is also stable in 10^{-3} atm O_2 to 1000 °C. In 10^{-4} and 10^{-5} atm oxygen, LSC64 was observed to decompose at 1000 and 950 °C, respectively. The decomposition products are $LaSrCoO_4$ and CoO. In both cases the decomposition phases persisted on cooling back to room temperature. The phase transition to the brownmillerite phase was not observed for LSC64 or LSC82 down to 10^{-5} atm oxygen; however, as will be shown later, the brownmillerite phases do form under reducing gas. This can be explained in terms of the vacancy concentrations in the starting materials: since LSC64 and LSC82 begin with significantly less Sr^{2+} ions than LSC37, the structure is closer to the $A^{3+}B^{3+}O_3$ parent compound and contains fewer oxygen vacancies. It appears that even partial ordering to form some

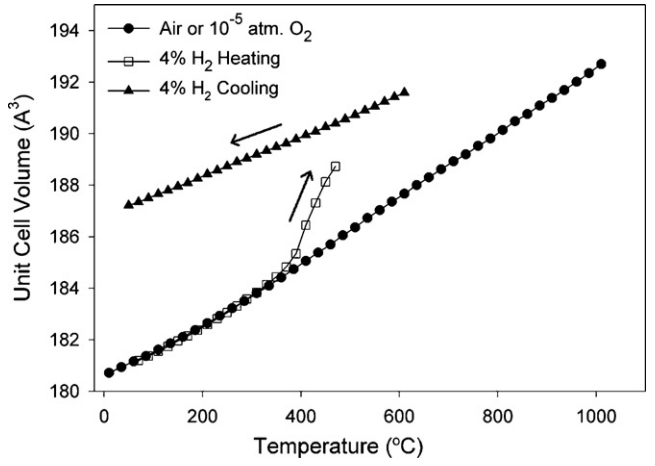

Fig. 8. Unit cell volume vs. temperature for $LaSrCoO_4$ and $LaSrCoO_{3.5}$ under 10^{-5} atm oxygen, air, and 4% H_2. Error bars are smaller than the symbols and not shown. Reduction of $LaSrCoO_4$ to $LaSrCoO_{3.5}$ is evident under H_2.

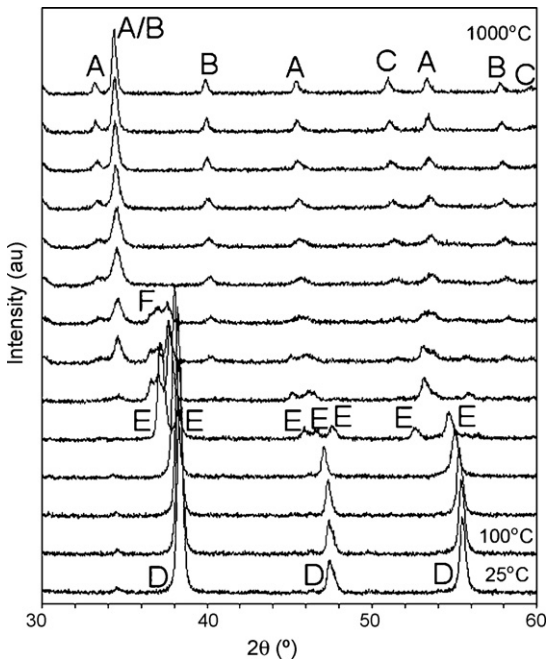

Fig. 9. *In situ* X-ray diffraction patterns (Co radiation, $\lambda = 1.79$ Å) for LSC64 heated in 4% hydrogen. Data are shown in steps of 75 °C. A = La_2O_3, B = SrO, C = Co, D = LSC64, E = vacancy-ordered oxygen deficient LSC64 and F = $SrLaCoO_4$.

fraction of the $ABO_{2.5}$ compound requires some minimum vacancy concentration, probably on the order of $\delta \sim 0.3$, a value between that of LSC37 and LSC64 [15].

In Fig. 9 we can see the effect of heating LSC64 in a reducing atmosphere. As with LSC37, LSC64 forms a brownmillerite phase in 4% H_2 at a relatively low temperature (250 °C), and then undergoes a disordering transition back to the cubic perovskite at 375 °C, at which temperature decomposition also begins and $LaSrCoO_4$ begins to form. Above 400 °C a second set of decomposition products begins to form (La_2O_3, SrO, and Co metal), and $LaSrCoO_4$ has reacted away by 600 °C. These products remain constant up to 1000 °C and through cooling to room temperature. Again, reheating the product in air at 1000 °C resulted in LSC64 reforming within minutes.

LSC82 is also rhombohedral at room temperature and is stable in oxygen partial pressures of 1% and 10^{-3} atm oxygen to 1000 °C. LSC82 is the most stable of the three compositions, with the first sign of decomposition to form $(La,Sr)_2CoO_4$ evident under 10^{-4} atm at 1000 °C, but only after holding for ~30 min. At 10^{-5} atm oxygen, LSC82 begins to decompose at 1000 °C within minutes.

The decomposition of LSC82 in 4% H_2 follows the same path as the other LSC samples. At 325 °C initial vacancy ordering occurs, but, unlike the LSC64, no vacancy disordering is observed before decomposition begins. At 550 °C, La_2O_3, SrO, and Co metal form, which persist to 1000 °C and back to room temperature. Again, reheating these products in air to 1000 °C results in reaction to form LSC82.

The stability at reduced oxygen pressure is a function of A-site chemistry for the LSC series studied. For example, at 10^{-5} atm oxygen, LSC37, LSC64, and LSC82 first decompose at 925, 950, and 1000 °C. The first appearance of the brownmillerite phase under H_2 follows the same trend, and occurs at ~200, 250, and 325 °C for LSC37, LSC64, and LSC82, respectively. This trend is attributed to the starting oxygen vacancy concentration, which increases with Sr content.

Some questions in the literature regarding the phase behavior of LSC at low oxygen pressures are clarified by careful

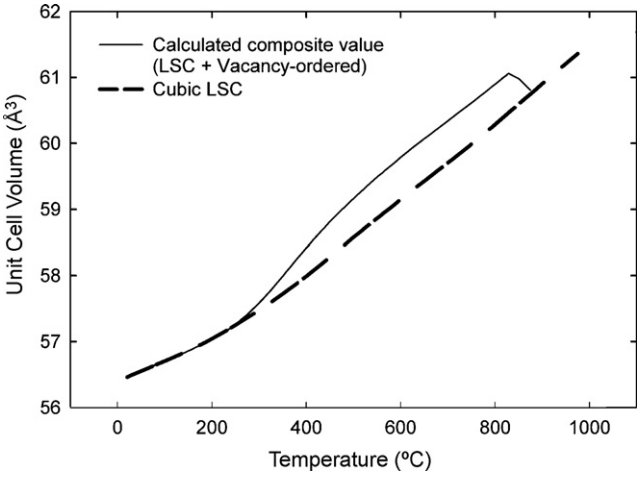

Fig. 10. Calculated composite unit cell volume and the unit cell volume for LSC37, demonstrating the overall decrease in density resulting from the presence of the vacancy-ordered phase.

examination of the *in situ* XRD data. Chen et al. [15] studied LSC37, LSC64, and LSC82 as a function of oxygen pressure over the range 10^{-4} atm < pO_2 < 0.21 atm using dilatometry. The authors noted a long-term drift, on the order of a few percent, in the measured sample lengths over the course of several days. In order to compare our results with those of Chen [15], we used the *in situ* diffraction data to estimate the sample size as a function of the degree of conversion to the vacancy-ordered LSC phase.

The two-phase system consisting of cubic LSC and orthorhombic vacancy-ordered LSC was treated as a composite with linear mixing. The orthorhombic cell was converted to an equivalent cubic unit cell, and the weight fractions of each phase were used to calculate the equivalent composite unit cell volume. Fig. 10 shows the result, demonstrating that the mass density of the vacancy-ordered phase is significantly lower that that of cubic LSC. Indeed, Rietveld analysis of the XRD data at 800 °C and 10^{-5} atm oxygen yield densities of 5.42 and 5.75 g cm^{-3} for the vacancy-ordered and LSC phases, respectively. It is interesting to note that the change in sample volume as a result of 10–50 wt% of the vacancy-ordered phase is on the order of one to a few percent. This magnitude of change in sample dimensions is in agreement with the long-term drifts detected by Chen [15] and therefore is the likely explanation for their observations.

4. Conclusions

The phase stability of $La_{1-x}Sr_xCoO_{3-\delta}$ has been shown to increase with decreasing x at high temperature and low oxygen partial pressure or under reducing conditions. A new vacancy-ordered phase has been observed *in situ*. The ordered phase develops on heating in low oxygen atmospheres, and adopts the brownmillerite structure. The vacancy-ordered phases disorder on heating, resulting in a vacancy ordering sequence of disordered → ordered → disordered. The onset of oxygen vacancy ordering is a function of oxygen content, with initial vacancy ordering under 4% H_2 occurring at 200, 250, and 325 °C for LSC37, LSC64, and LSC82, respectively. All three materials decompose when held in pO_2 as low as 10^{-5} atm by 1000 °C, to form $(SrLa)_2CoO_4$ as a primary decomposition product. Again, stability is higher with increasing La content. Under reducing conditions of 4% H_2, $(SrLa)_2CoO_4$ transforms to $(La,Sr)_2CoO_{3.5}$, which has a substantially lower CTE than the stoichiometric phase.

Acknowledgements

SM thanks Stu Adler at the University of Washington for useful discussions. This work was supported in part by the New York State Foundation for Science, Technology and Innovation, NYSTAR, under contract C030093. Research at beam line X14A, NSLS, sponsored by the Assistant Secretary for Energy Efficiency and Renewable Energy, Office of FreedomCAR and Vehicle Technologies, as part of the High Temperature Materials Laboratory User Program, Oak Ridge National Laboratory, managed by UT-Battelle, LLC, for the U.S. Department of Energy under contract number DE-AC05-00OR22725.

References

[1] K. Tsutsui, J. Inoue, S. Maekawa, Phys. Rev. B 59 (1999) 4549.
[2] H.W. Hsu, Y.H. Chang, G.J. Chen, K.J. Lin, Mater. Sci. Eng. B 64 (1999) 180–186.
[3] A.N. Petrov, O.F. Kononchuk, A.V. Andreev, V.A. Cherepanov, P. Kofstad, Solid State Ionics 80 (1995) 189–199.
[4] K.S. Lee, S. Lee, J.W. Kim, S.K. Woo, Desalination 147 (2002) 439–444.
[5] V.V. Kharton, E.V. Tsipis, A.A. Yaremchenko, I.P. Marozau, A.P. Viskup, J.R. Frade, E.N. Naumovich, Mater. Sci. Eng. B 134 (2006) 80–88.
[6] R.H.E. van Doorn, A.J. Burggraaf, Solid State Ionics 128 (2000) 65–78.
[7] Y. Liu, L. Hong, J. Membr. Sci. 224 (2003) 137–150.
[8] N.P. Bansal, Z. Zhong, J. Power Sources 158 (2006) 148–153.
[9] H. Kurokawa, C.P. Jacobson, L.C. DeJonghe, S.J. Visco, Solid State Ionics 178 (2007) 287–296.
[10] Y. Zhu, H. Wang, R. Tan, L. Cao, J. Alloys Compd. 352 (2003) 134–139.
[11] M. Sase, J. Suzuki, K. Yashiro, T. Otake, A. Kaimai, T. Kawada, J. Mizusaki, H. Yugami, Solid State Ionics 177 (2006) 1961–1964.
[12] J. Ovenstone, C.B. Ponton, Br. Ceram. Proc. 58 (1998) 155–163.
[13] J. Ovenstone, C.B. Ponton, J. Mater. Sci. 35 (2000) 4115–4119.
[14] E. Bucher, W. Sitte, I. Rom, I. Papst, W. Grogger, F. Hofer, Solid State Ionics 152/153 (2002) 417–421.
[15] X. Chen, Chem. Mater. 17 (2005) 4537–4546.
[16] E. Girdauskaite, H. Ullmann, V. Vashook, M. Bulow, U. Guth, Solid State Ionics 177 (2006) 1831–1835.
[17] H. Huang, Preparation, electrical properties and phase compatibility studies of $La_{1-x}Sr_xCoO_3$ for electrode applications in ceramic multilayer devices, Alfred University M.S. Thesis (1999).
[18] A. Mineshige, M. Inaba, T. Yao, Z. Ogumi, K. Kikuchi, M. Kawase, J. Solid State Chem. 121 (1996) 423–429.
[19] A. Mineshige, M. Kobune, S. Fujii, Z. Ogumi, M. Inaba, T. Yao, K. Kikuchi, J. Solid State Chem. 142 (1999) 374–381.
[20] F. Morin, G. Trudel, Y. Denos, Solid State Ionics 96 (1997) 129–139.
[21] V. Sikolenko, A. Sazonov, V. Efimov, V. Krivencov, N. Darowski, D. Vyalikh, J. Mag. Mag. Mater. 310 (2007) e181–e183.
[22] W. Sitte, E. Bucher, A. Benisek, W. Preis, Spectrochim. Acta A: Mol. Biomol. Spectrosc. 57 (2001) 2071–2076.
[23] M. Sogaard, P.V. Hendriksen, M. Mogensen, F.W. Poulsen, E. Skou, Solid State Ionics 177 (2006) 3285–3296.
[24] C. Zhang, B.H. Kim, J.S. Kim, Y.W. Park, Phys. Lett. A 348 (2005) 58–65.
[25] A. Petrov, V. Cherepanov, A. Zuev, J. Solid State Electrochem. 10 (2006) 517–537.
[26] S. Misture, J. Electroceram. 16 (2006) 167–178.
[27] R. Caciuffo, D. Rinaldi, G. Barucca, J. Mira, J. Rivas, M.A. Señarís-Rodríguez, P.G. Radaelli, D. Fiorani, J.B. Goodenough, Phys. Rev. B 59 (1999) 1068.
[28] R.F. Klie, Y. Ito, S. Stemmer, N.D. Browning, Ultramicroscopy 86 (2001) 289–302.
[29] U. Bangert, U. Falke, A. Weidenkaff, Mater. Sci. Eng. B 133 (2006) 30–36.
[30] S. Stemmer, A. Sane, N.D. Browning, T.J. Mazanec, Solid State Ionics 130 (2000) 71–80.
[31] R.H.E. van Doorn, H.J.M. Bouwmeester, A.J. Burggraaf, Solid State Ionics 111 (1998) 263–272.
[32] F. Prado, N. Grunbaum, A. Caneiro, A. Manthiram, Solid State Ionics 167 (2004) 147–154.
[33] L.M. Liu, T.H. Lee, L. Qiu, Y.L. Yang, A.J. Jacobson, Mater. Res. Bull. 31 (1996) 29–35.
[34] N. Grunbaum, L. Mogni, F. Prado, A. Caneiro, J. Solid State Chem. 177 (2004) 2350–2357.
[35] V.V. Vashook, M.V. Zinkevich, Y.G. Zonov, Solid State Ionics 116 (1999) 129–138.
[36] M. James, T. Tedesco, D.J. Cassidy, R.L. Withers, Mater. Res. Bull. 40 (2005) 990–1000.
[37] S.T. Misture, Meas. Sci. Technol. 14 (2003) 1091–1098.
[38] International Centre for Diffraction Data Powder Diffraction File [CD-ROM]. Newtown Square, PA. Set 47, 2007.
[39] Inorganic Crystal Structure Database [CD_ROM], Fachinformationszentrum, 2007.
[40] K.H. Ryu, K.S. Roh, S.J. Lee, C.H. Yo, J. Solid State Chem. 105 (1993) 550–560.
[41] M.A. Hayward, M.J. Rosseinsky, Chem. Mater. 12 (2000) 2182–2195.